UC Davis
UC Davis Previously Published Works

Title

Targeting stroma and tumor, silencing galectin 1 treats orthotopic mouse hepatocellular carcinoma.

Permalink

Journal

ISSN

Authors

Setayesh, Tahereh
Hu, Ying
Vaziri, Farzam
et al.

Publication Date

DOI

ORIGINAL ARTICLE

Targeting stroma and tumor, silencing galectin 1 treats orthotopic mouse hepatocellular carcinoma

Tahereh Setayesh[a], Ying Hu[a], Farzam Vaziri[a], Xin Chen[b],
Jinping Lai[c], Dongguang Wei[a], Yu-Jui Yvonne Wan[a,*]

[a]Department of Medical Pathology and Laboratory Medicine, University of California, Davis, Sacramento, CA 95817, USA
[b]Cancer Biology Program, the University of Hawaii Cancer Center, Honolulu, HI 96813, USA
[c]Department of Pathology and Laboratory Medicine, Kaiser Permanente Sacramento Medical Center, Sacramento, CA 95825, USA

Abstract   This study examines inhibiting galectin 1 (Gal1) as a treatment option for hepatocellular carcinoma (HCC). Gal1 has immunosuppressive and cancer-promoting roles. Our data showed that Gal1 was highly expressed in human and mouse HCC. The levels of Gal1 positively correlated with the stages of human HCC and negatively with survival. The roles of Gal1 in HCC were studied using overexpression (OE) or silencing using *lgals1* siRNA delivered by AAV9. Prior to HCC initiation induced by RAS and AKT mutations, *lgals1*-OE and silencing had opposite impacts on tumor load. The treatment effect of *lgals1* siRNA was further demonstrated by intersecting HCC at different time points when the tumor load had already reached 9% or even 42% of the body weight. Comparing spatial transcriptomic profiles of Gal1 silenced and OE HCC, inhibiting matrix formation and recognition of foreign antigen in CD45^{+} cell-enriched areas located at tumor-margin likely contributed to the anti-HCC effects of Gal1 silencing. Within the tumors, silencing Gal1 inhibited translational initiation, elongation, and termination. Furthermore, Gal1 silencing increased immune cells as well as expanded cytotoxic T cells within the tumor, and the anti-HCC effect of *lgals1* siRNA was CD8-dependent. Overall, Gal1 silencing has a promising potential for HCC treatment.

*Corresponding author.
  E-mail address: yjywan@ucdavis.edu (Yu-Jui Yvonne Wan).

1. Introduction

Hepatocellular carcinoma (HCC) is a leading cause of cancer-related death globally, and early detection and effective treatment options are limited[1]. Current therapies for advanced-stage HCC only offer modest clinical benefits and are associated with various side effects, resulting in a median survival time of about a year[2,3]. To overcome these limitations, novel approaches are urgently needed to target the molecular drivers of HCC and shut down pathological signaling.

Galectin1 (Gal1) is a carbohydrate-binding lectin that interacts with glycoconjugate ligands of the extracellular matrix, endothelial cells, and T lymphocytes[4–8]. Gal1 is overexpressed in many types of cancers (e.g., liver, colon, breast, and lung) and is involved in multiple aspects of tumorigenesis, including cell proliferation, invasiveness, metastasis, and angiogenesis[9–12]. One known mechanism by which Gal1 promotes tumor growth is to induce epithelial to mesenchymal transition (EMT), a critical step for tumor initiation and being invasive[13,14]. Moreover, Gal1 can lead to the development of sorafenib-resistant cells through the activation of the PI3K/AKT signaling pathway[15,16]. Thus, Gal1 can be a target for cancer therapeutics. Surprisingly, using multidrug-resistance 2 and Gal1 double knockout mice, loss of Gal1 increases hepatic injury, inflammation, and fibrosis[17]. It is likely that silencing Gal1 in the germline can lose its immuno-suppressive protective role and make the double knockout mice more susceptible to liver injury. Thus, the roles of Gal1 in HCC remain to be characterized.

Using xenograft models, a combination of a Gal1 inhibitor, OTX008, and sorafenib significantly reduced tumor growth[13]. However, in 2012, a phase 1 clinical trial was conducted to evaluate the effect of OTX008 to treat advanced solid tumors (ClinicalTrials.gov: NCT01724320). The data showed that OTX008 reduced serum Gal1 but with side effects. So far, the outcome of the study has not been released. Thus, there is a need to develop an effective, stable, and safe approach to inhibiting Gal1. Moreover, emerging evidence revealed the significance of gut microbiome and immunity in influencing liver health[18,19]. Therefore, it is also important to study liver carcinogenesis and treatment using orthotopic mouse models.

The current study examines the efficacy of gene therapy to silence Gal1 in HCC treatment using orthotopic preclinical models. Adeno-associated virus (AAV) serotype 9, which has been demonstrated to be safe in 263 clinical trials, was used to deliver Gal1 for overexpression or silencing[20]. Our data revealed that Gal1 overexpression prior to tumorigenesis facilitated liver carcinogenesis, while silencing it could prevent and treat HCC as well as prolong survival. Mechanistically, Gal1 silencing acts on several pathways based on locations. Those pathways included regulating translation machinery within the tumor, reducing the interactions between CD45$^+$ cells and matrix formation at the tumor margin, shifting T cell populations, etc. In addition, the HCC treatment effect of Gal1 silencing was cytotoxic T cell dependent. Together, the generated data demonstrated promising outcomes for both preventative and therapeutic applications of AAV9-mediated Gal1 silencing, which selectively targets stromal and tumor cells and exhibited no observable toxicity in preclinical models.

2. Material and methods

2.1. Clinical specimens

Frozen liver cancers ($n = 11$) and normal livers ($n = 9$), confirmed by histological evaluation, were obtained from the Translational Pathology Core Laboratory Shared Resource at the University of California, Los Angeles (UCLA, CA, USA). Among them, six tumors and adjacent normal tissues were paired and derived from six HCC patients. The tissue procurement process was approved by the UCLA Institutional Review Board with protocol number 11-2504 approved on 1 February 2011. A microarray slide consisting of 22 HCC specimens was obtained from the UC Davis Pathology Biorepository at UC Davis Health under the UC Davis Comprehensive Cancer Center.

The human tissue procurement process was approved by the UCLA Institutional Review Board with protocol number 11-2504 approved on 1 February 2011.

2.2. Generating HCC mouse models and treatment strategies

Wild-type male and female FVB/N mice were obtained from the Jackson Laboratories (Sacramento, CA, USA) and were housed in regular filter-top cages at 22 °C with a 12 h:12 h light cycle. For hydrodynamic injection, myr-Akt1 and N-RasV12 (1 µg/g body weight) and sleeping beauty transposase plasmid (0.08 µg/g body weight) were diluted in 2 mL PBS filtered (0.22 µm) and injected into the lateral tail vein of 6 weeks-old mice in 7 s. Constructs used in these animal experiments showed long-term expression of genes via a hydrodynamic injection[21]. Animal experiments were conducted following the National Institutes of Health Guide for the Care and Use of Laboratory Animals under protocols approved by the Institutional Animal Care and Use Committee of the University of California, Davis, CA, USA.

To silence the Gal1, AAV9 (Applied biological material, Richmond, BC, Canada) was used. Target sequences were: target a—81:CGCCAAGAGCTTTGTGCTGAA, target b—178:GTGTGTAACACCAAGGAAGAT, target c—306:AGACGGACATGAATTCAAGTT, and target d—367:GCGGATGGAGACTTCAAGATTAAGTGCGT. The vector size was 6593 bp (Supporting Information Fig. S1A). The vector was tagged with GFP. Gal1 siRNA (10^{12} genome copy/kg BW) was administered intravenously once. Scramble-AAV9 was used as a control. The same vector was used to overexpress the Gal1, 10^{12} genome copy/kg BW (Fig. S1B). Blank AAV9 was administered as a control (Fig. S1C).

To understand how immune cells are involved in the therapeutic effects of lgals1 siRNA, CD8 was depleted in mice by i.p. injection of 200 µg/kg body weight of either anti-mouse CD8α (BE0004-1; Bioxcell) or isotype control (BE0089; Bioxcell) two times a week for 3 consecutive weeks.

2.3. Histology and immunohistochemistry

Tissues were fixed in 10% formalin for 16 h and kept in 70% ethanol for 72 h, followed by embedding in paraffin and cutting into 5-μm sections. Hematoxylin and eosin (H&E) staining was performed[22]. Mouse tumor score was quantified by pathologists based on H&E stained slides using five criteria (i.e., the level of centrilobular vacuolar degeneration, the number of proliferation foci, scirrhous type foci of proliferation mitotic index, and inflammatory cells)[23,24]. Details are described in Supporting Information Table S1.

Immunostaining was performed with specific antibodies against Gal1 (Abcam, Cambridge, MA, USA) and CD8 (eBioscience, Waltham, MA). The number of positive-staining cells was counted in at least five random microscopic fields (100 × magnification) for each section.

2.4. In situ apoptosis analysis

Terminal deoxynucleotidyl transferase dUTP nick end labeling (TUNEL) assay kit (Abcam, Cambridge, MA, USA) was used. Liver sections were incubated with 3% H_2O_2 to inactivate endogenous peroxidases after being treated with proteinase K. Biotin labeling of DNA-exposed 3′-OH ends of apoptotic cells was produced by adding terminal deoxynucleotidyl transferase (TdT) enzyme, and TdT labeling reaction mix. Biotinylated DNA was detected by incubation (30 min) with a streptavidin−HRP conjugate. After washing in TBS, DAB substrate was added, and reactions were stopped. The sections were counterstained with Methyl Green, dehydrated, and then coverslipped. Images were taken under a Nikon Eclipse E600 microscope. The number of apoptotic cells was determined by counting positive-staining cells in at least five random microscopic fields (100 × magnification) for each specimen.

2.5. Measurement of biochemical parameters and cytokines

Serum samples were used to detect alanine aminotransferase, aspartate transferase, cholesterol, lipase, and creatine kinase by colorimetric method slide based on published methods (Fujifilm DRI-CHEM SLIDE)[25]. Mouse interferon-gamma (IFN-γ) and granzyme B were quantified using the ELISA kits (Abcam, MA, USA). To evaluate the collagen content, hepatic hydroxyproline concentration was determined using the colorimetric assay kit (Sigma−Aldrich).

2.6. RNA isolation, quantitative real-time PCR

RNA was extracted using a TRIzol reagent (Thermo Fisher Scientific, Waltham, MA, USA). cDNA was synthesized using a high-capacity RNA-to-cDNA kit (Applied Biosystems, Carlsbad, CA, USA). Real-time quantitative PCR with reverse transcription (RT-qPCR) was performed on a QuantoStudio5, applied biosystems by Thermo Fisher scientific system using Power SYBR Green PCR master mix (Life Technologies). Primers were designed using Primer3 Input software version 0.4.0. The glyceraldehyde-3-phosphate dehydrogenase (Gapdh) mRNA level served as an internal control. Data generated from healthy livers were used to establish a baseline to calculate the relative expression levels between groups. The relative mRNA level was calculated by the $2^{-\Delta\Delta CT}$ method.

2.7. RNA sequencing and functional analysis

RNA quality control was performed using Qubit and Bioanalyzer instruments. Libraries were prepared using the NEBNext Ultra II non-directional RNA Library Prep kit. Library quality and concentration were assessed with Labchip and qPCR and subjected to sequencing using Novaseq6000. Differential expression analysis of two conditions/groups (two biological replicates per condition) was performed using the DESeq2 R package (1.20.0). DESeq2 provides statistical routines for determining differential expression in digital gene expression data using a model based on the negative binomial distribution. The resulting P-values were adjusted using Benjamini and Hochberg's approach for controlling the false discovery rate. Genes with an adjusted P-value. The DEGs were used for KEGG analyses using the cluster profile package[25], and an adjusted P-value of <0.05 was considered a significant event. Moreover, Gene set enrichment analysis (GSEA) was utilized to discover the molecular mechanism of the whole genome at the transcription level rather than the DEGs.

2.8. GeoMx DSP whole transcriptome workflow

Liver sections (4 μm) were used for digital spatial profiler (DSP) whole transcriptome sequencing (NanoString). The panel of morphology markers used included CD45 in addition to SYTO13 nuclear stain and Pan-cytokeratin. Slides were stained with RNAscope probes and GeoMx DSP oligo-conjugated RNA detection probes according to manufacture protocol.

Slides were loaded onto the GeoMX DSP slide holder with 6 mL of Buffer S (GeoMx RNA slide prep kit, Nanostring). Files were configured to associate RNA targets and GeoMx readout barcodes. The appropriate scan type and focus channel were selected to populate fluorescence exposure settings. Scan areas were defined for high magnification. A total of 8 regions of interest (ROIs) with a diameter of 300−600 μm per group were selected (4 tumors and 4 margins). The Geomx software was used to define the area of illumination within each ROI, was further segmented based on morphological markers (CD45, SYTO13, and PanCK), followed by UV-cleaved DSP barcodes from each ROI, were collected, dispensed into a 96-well plate, and counted. These barcodes were tagged with their specific RNA target identification sequence and ROI location during library preparation; therefore, can be matched to their in situ hybridization probes and the unique molecular identifier for read deduplication. The sequenced oligonucleotides were then imported into the GeoMx DSP platform to be integrated with slide images and ROI selections for spatially resolved RNA expression. The FASTQ sequencing files were converted into digital count files using Nanostring's GeoMx NGS Pipeline software. Quality control checks and data analysis were performed using the GeoMx DSP Data Analysis suite. The data were filtered by the limit of quantitation and then normalized by the third quartile of all counts. Cell deconvolution analyses were performed using the spatialdecon geoscript (v1.3 updated October 2022) available at Nanostring's Geoscript Hub.

2.9. Cell deconvolution analyses

The spatialdecon geoscript (v1.3 updated October 2022) available at Nanostring's Geoscript Hub was used to generate cell deconvolution analyses in the GeoMx DSP control center [https://nanostring.com/products/geomx-digital-spatial-profiler/geoscript-hub/].

The abundance of immune cells (*e.g.*, CD8 T cell) was calculated based on the single sample GSEA enrichment score of the expression deviation profile per cell type[26,27]. Subsequently, the calculated enrichment score was normalized, which is used as the abundance of immune cells (http://bioinfo.life.hust.edu.cn/web/ImmuCellAI/).

2.10. Bioinformatics analysis of human HCC

Normalized mRNA data for liver hepatocellular carcinoma (LIHC) were obtained from the University of California, Santa Cruz (UCSC) Xena browser (https://xenabrowser.net/). Univariate and bivariate expression analyses among cases were performed with the R software. To further explore the prognostic value of the gene-expression signature driven by *lgals1* (high or low), cancer patients were divided into two subgroups for survival analyses. Discretization of the *lgals1* gene expression data into low- or high-expression levels was performed according to the StepMiner one-step algorithm (http://genedesk.ucsd.edu/home/public/StepMiner/). These two groups were then compared for overall survival and disease-specific survival (Kaplan−Meier curves and log-rank test) using the survival and survminer R packages.

2.11. Statistical analysis

All quantitative data are expressed as mean ± standard error of mean (SEM). Groups were compared using one-way ANOVA followed by a Tukey test. Mann−Whitney test was used to compare two groups. Survival curves were plotted by Kaplan−Meier analysis and compared using the log-rank test. All analyses were carried out using the GraphPad Prism 9.0 statistical software package (San Diego, CA, USA), and *P* values < 0.05 were considered significant.

3. Results

3.1. Gal1 is overexpressed in human and mouse HCC

Histological normal human livers ($n = 9$) had low levels of *LGALS1* mRNA in comparison with human HCCs ($n = 11$) revealed by real-time PCR. Among those specimens, six paired specimens were obtained from the same HCC patients (Fig. 1A). The findings were confirmed by immunohistochemistry (IHC) using another cohort of 22 specimens from HCC patients. The number of Gal1-positive cells was quantified using ImageJ. In human HCC, about 80% of cells demonstrated high immunoreactivity of Gal1 (Fig. 1B).

In consistency, analysis of the data available in the Cancer Genome Atlas (TCGA) revealed that the expression levels of *LGALS1* were significantly higher in HCC ($n = 371$) compared to normal livers ($n = 50$) (Fig. 1C). In addition, patients with HCC who exhibited high levels of *LGALS1* had a shorter overall survival rate compared to those with low expression levels of *LGALS1* ($P = 0.0298$) (Fig. 1D). Furthermore, there was a significant increase in *LGALS1* mRNA levels observed in stage 2 and 3 HCCs compared to stage 1 tumors (Fig. 1E).

Similar findings were observed in oncogenes Akt/Ras-induced mouse HCC. *Lgals*1 mRNA levels were much higher in mouse HCCs than in healthy livers (38-fold difference, $n = 8$/group) (Fig. 1F), and the data were validated by IHC (Fig. 1G). Together, elevated Gal1 was found in both human specimens from different sources as well as preclinical mouse HCC models.

3.2. Gal1 silencing attenuates carcinogenesis, while overexpression of Gal1 accelerates tumorigenesis

Gal1 silencing and overexpression (OE) were initiated 3 days prior to tumor initiation using oncogenes Akt and Ras delivered by hydrodynamic injection (Fig. 2A). There were no differences in liver histology, the liver-to-body weight (L/BW) ratio, and spleen weight of HCC mice that received either scramble-AAV9 or blank-AAV9 compared with untreated HCC mice (Fig. 2B and C). Those groups are referred to as "HCC mice" in the manuscript. The study design generated HCC-bearing mice that had an L/BW ratio of ∼25% in contrast to ∼4.5% found in healthy mice. The silencing of Gal1 reduced the L/BW to ∼10% in contrast to increasing it to ∼33%, caused by *lgals1*-OE (Fig. 2B). Because interventions were introduced prior to the tumor initiation, the findings suggested that silencing Gal1 prevents HCC development and that OE Gal1 promotes it.

HCC patients with splenomegaly have a worse survival outcome, and splenectomy improves the long-term survival of those patients[28]. HCC mice also had splenomegaly, which was 3 times larger than that of healthy mice. The splenomegaly found in HCC mice was reduced by Gal1 silencing as well (Fig. 2C).

Morphologically, HCC mice and *lgals1*-OE livers had multiple large nodules featuring steatosis, fibrosis, and multiple Mallory bodies, and Gal1 silencing was very effective in reducing the size of tumors as well as improving other pathological features (Fig. 2D and E). Histological scoring was evaluated based on the levels of centrilobular vacuolar degeneration, foci of proliferation, mitotic rate, scirrhous type of foci of proliferation, and inflammatory cell infiltration (Table S1). The overall histological scores are summarized in Fig. 2F.

Excitingly, Gal1 silencing significantly reduced fibrosis quantified by hydroxyproline assay (Fig. 2G). Furthermore, the mRNA levels of HCC markers (*Lgals1*, *Afp*, and *Ezh2*) and fibrosis markers (*α-Sma*, *Tgf-β*, and *Vimentin*) were significantly upregulated in HCC, and further increased due to *lgals1*-OE, and Gal1 silencing reversed them (Fig. 2H).

3.3. Gal1 silencing treats HCC, and improves overall survival

The HCC treatment effect of AAV9-*lgals1* siRNA was studied by intersecting the tumors at different times. The interventions were initiated 7- and 44-days post-tumor initiation when the L/BW ratios reached 9% and 40%, respectively. In addition, a survival study was performed in both sexes.

Silencing Gal1, 7 days post tumor initiation, normalized the L/BW demonstrated in HCC mice of both sexes (Fig. 3A). There was no difference in L/BW of the healthy mice and Gal1 silenced HCC mice (Fig. 3B). GFP-tagged *lgals1* siRNA-AAV9 was highly visible in the liver, confirming liver tropism (Fig. S1D). The HCC mice treated with *lgals1* siRNA had a reduction in L/BW ratio (by 83%) and spleen weight (by 44%) compared to HCC mice (Fig. 3B and C). HCC mice of both sexes displayed numerous prominent tumor nodules accompanied by fibrosis and the presence of multiple Mallory bodies. Notably, suppression of Gal1 expression was highly effective in reducing the tumor load (Fig. 3D) and improving pathological characteristics (Table S1).
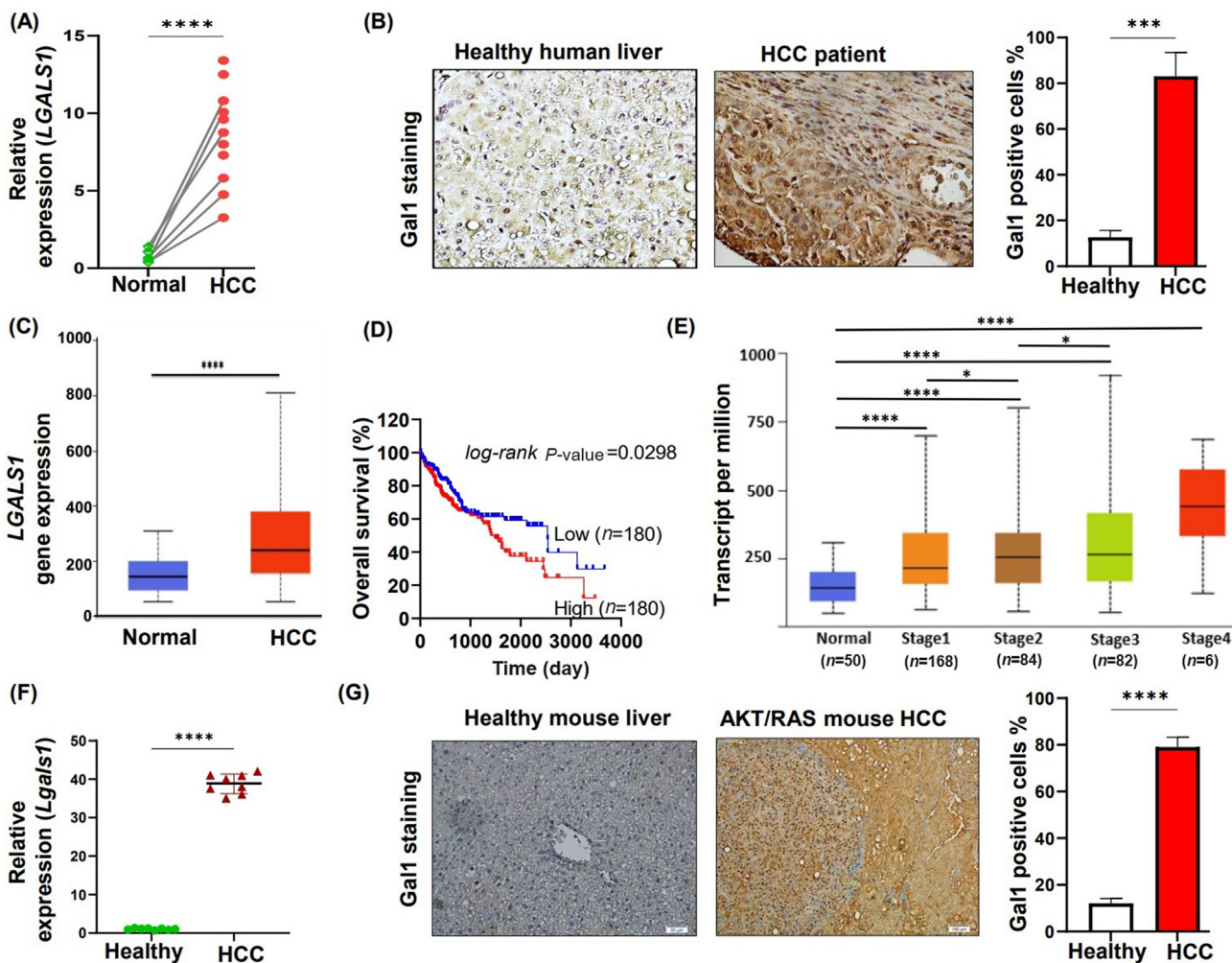
Figure 1   Gal1 is overexpressed in human and mouse HCC. (A) mRNA levels of *LGALS1* in tumors ($n = 11$) and histological normal livers ($n = 9$) of HCC patients. Among them, six tumors and adjacent normal tissues were paired, *i.e.*, derived from the same patients. (B) Representative Gal1 immunohistochemistry staining in a healthy human liver and HCC patient; percentage of Gal1 positive cells were counted in 5 random fields. Data are shown as mean ± SD. (C) The Cancer Genome Atlas (TCGA) data analysis shows elevated *LGALS1* expression in human HCCs ($n = 370$) compared to normal livers ($n = 50$). (D) Kaplan−Meier analysis of overall survival of patients with HCC according to *LGALS1* expression levels ($n = 360$ patients, TCGA data set, $P = 0.0298$). (E) Gal1 transcript per million in different stages of HCC; normal ($n = 50$), stage 1 ($n = 168$), stage 2 ($n = 84$), stage 3 ($n = 82$), and stage 4 ($n = 6$). (F) mRNA levels of *Lgals1* in healthy mouse livers and Akt/Ras-induced HCCs Data are shown as mean ± SD ($n = 8$). (G) Representative Gal1 immunohistochemistry staining in a normal liver and Akt/Ras-induced mouse HCC; percentage of Gal1 positive cells were counted in 5 random fields. Data are shown as mean ± SD ($n = 4$). *t*-Test and ANOVA were used, Tukey; *$P < 0.05$; **$P < 0.01$; ***$P < 0.001$; ****$P < 0.0001$.

The computed histological scores are shown in Supporting Information Fig. S2.

Furthermore, IHC staining in HCC mice treated with *lgals1* siRNA showed a reduction of Gal1 as well as Ki67 positive cells compared to untreated HCC or *lgals1*-OE treated HCC mice (Supporting Information Fig. S3). Further, serum alanine transaminase, aspartate aminotransferase, and cholesterol were reduced by *lgals1* siRNA treatment revealing improved liver function. Moreover, serum lipase concentration was neither changed by HCC development nor by Gal1 silencing. Serum creatine kinase, which was markedly increased due to HCC formation, was normalized by *lgals1* siRNA treatment, suggesting improved digestive function including the function of the pancreas (Supporting Information Fig. S4A−S4C).

To evaluate the potential toxicity of the *lgals1* siRNA treatment in HCC mice, additional biochemistry assays were performed. Serum lipase concentration remained in a normal range, indicating no pancreatic damage (Fig. S4D). Creatine kinase, a biomarker to judge the severity of muscle damage, was increased in HCC mice but normalized by *lgals1* siRNA treatment (Fig. S4E). Complete blood counts showed that HCC mice had increased white blood cells, granulocytes, percentage of lymphocytes, and monocytes but reduced hematocrit and mean corpuscular volume, among other abnormalities. In contrast, in response to *lgals1* siRNA treatment, all those changes were normalized. Thus, the data not only showed the benefits of Gal1 silencing but also demonstrated that AAV9-mediated gene therapy did not induce toxicity (Supporting Information Table S2).
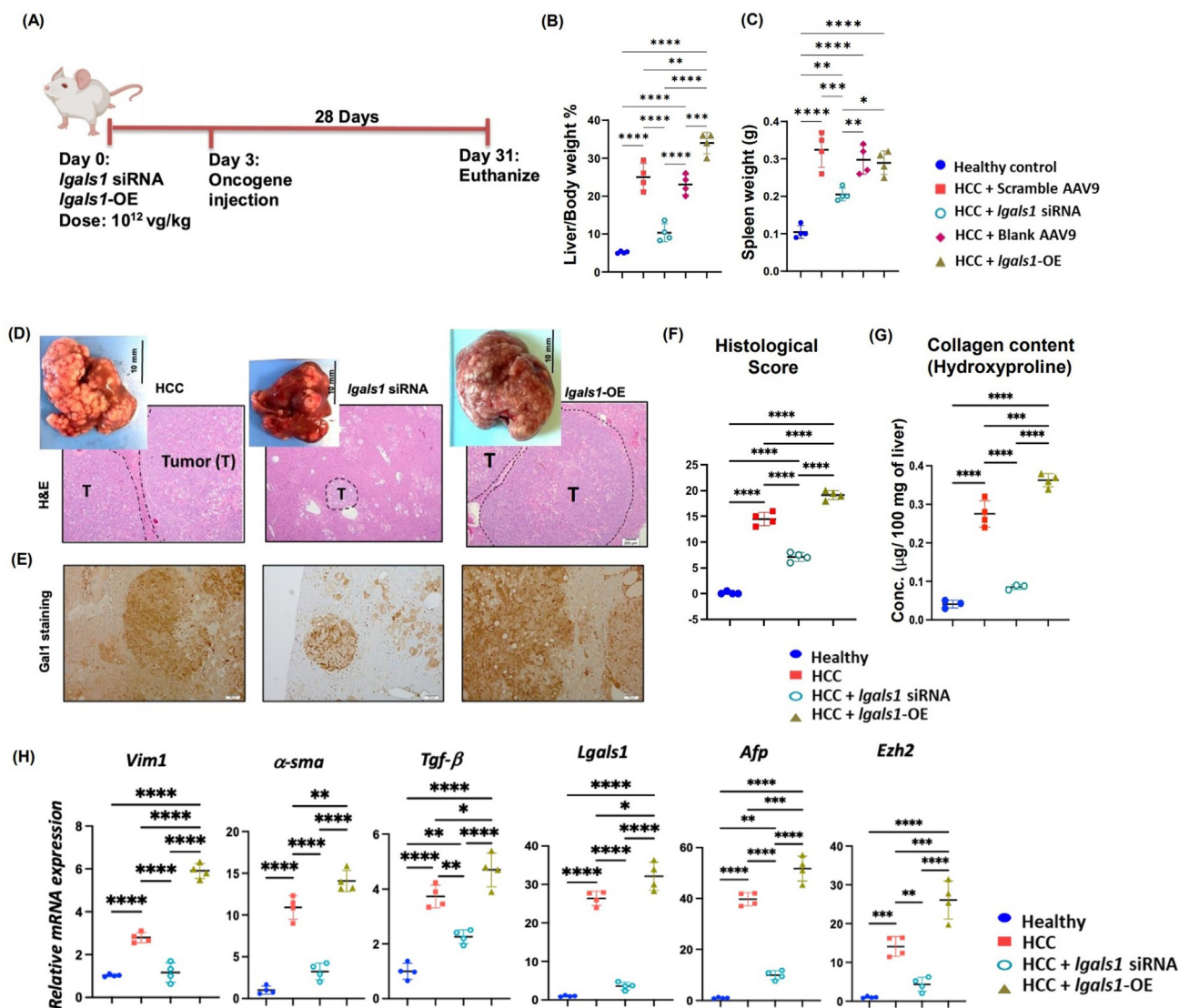
Figure 2 Gal1 silencing attenuates carcinogenesis, while overexpression of Gal1 accelerates tumorigenesis. (A) Experimental scheme. Gal1 silenced by i.v. injection of *lgals1* siRNA-AAV9 (*lgals1* siRNA) or overexpressed by i.v. injection of *lgals1*-AAV9 (*lgals1*-OE) (10^{12} genome copy/kg BW), which took place 3 days prior to oncogene injection. Control HCC mice received either scramble AAV9 or blank AAV9. Mice were euthanized 31 days after *lgals1* treatments. (B) Liver to body weight ratio. (C) Spleen weight. (D) Representative liver gross morphology and H&E-stained liver sections. (E) Gal1 immunohistochemistry staining. (F) Histological scores were quantitively evaluated based on criteria detailed in Table S1. (G) Liver fibrosis was measured by hepatic hydroxyproline assay. (H) Relative mRNA levels. Data are shown as mean $\pm$ SD (n = 4/group). ANOVA, Tukey, was used; *$P < 0.05$; **$P < 0.01$; ***$P < 0.001$; ****$P < 0.0001$.

Survival study uncovered that Gal1 silencing extended the survival time in both sexes (Fig. 3E). No significant differences (based on Log-rank, Mantel−Cox test) were observed in overall survival between female and male HCC mice treated with *lgals1* siRNA (Fig. 3E).

TUNEL assay was used to detect apoptotic cells that underwent DNA degradation[29]. The apoptotic cells were mainly found in the tumor area of *lgals1* siRNA treated mice (Fig. 3F). HCC mice had a median survival of 45 days (Fig. 3E).

We further studied whether silencing Gal1 would effectively inhibit tumor growth prior to the anticipated death time by introducing *lgals1* siRNA 44 days post-tumor initiation (Fig. 3G). By 57 days, untreated HCC, which remained alive, reached moribund and had to be euthanized, and those mice had an L/BW

ratio of ∼47%. Thus, the tumor load was almost half of the body weight. In contrast, by 57 days, *lgals1* siRNA treated mice were all actively alive, and they had an L/BW ratio of ∼38%, which was even lower than the baseline (42%), *i.e.*, when the intervention was introduced (Day 44) (Fig. 3H). Additionally, Gal1 silencing reduced the mRNA levels of proliferation marker *Mki67*, HCC marker Glypican 3 (*Gp3*), as well as *Lgals1* (Fig. 3I, Supporting Information Fig. S5).

3.4. Gal1 silencing inhibits HCC pathways

Gal1 targeted signaling was studied using different approaches. Transcriptomic profiles were compared using bulk liver RNA of healthy, HCC, and HCC mice treated with *lgals1* siRNA, or
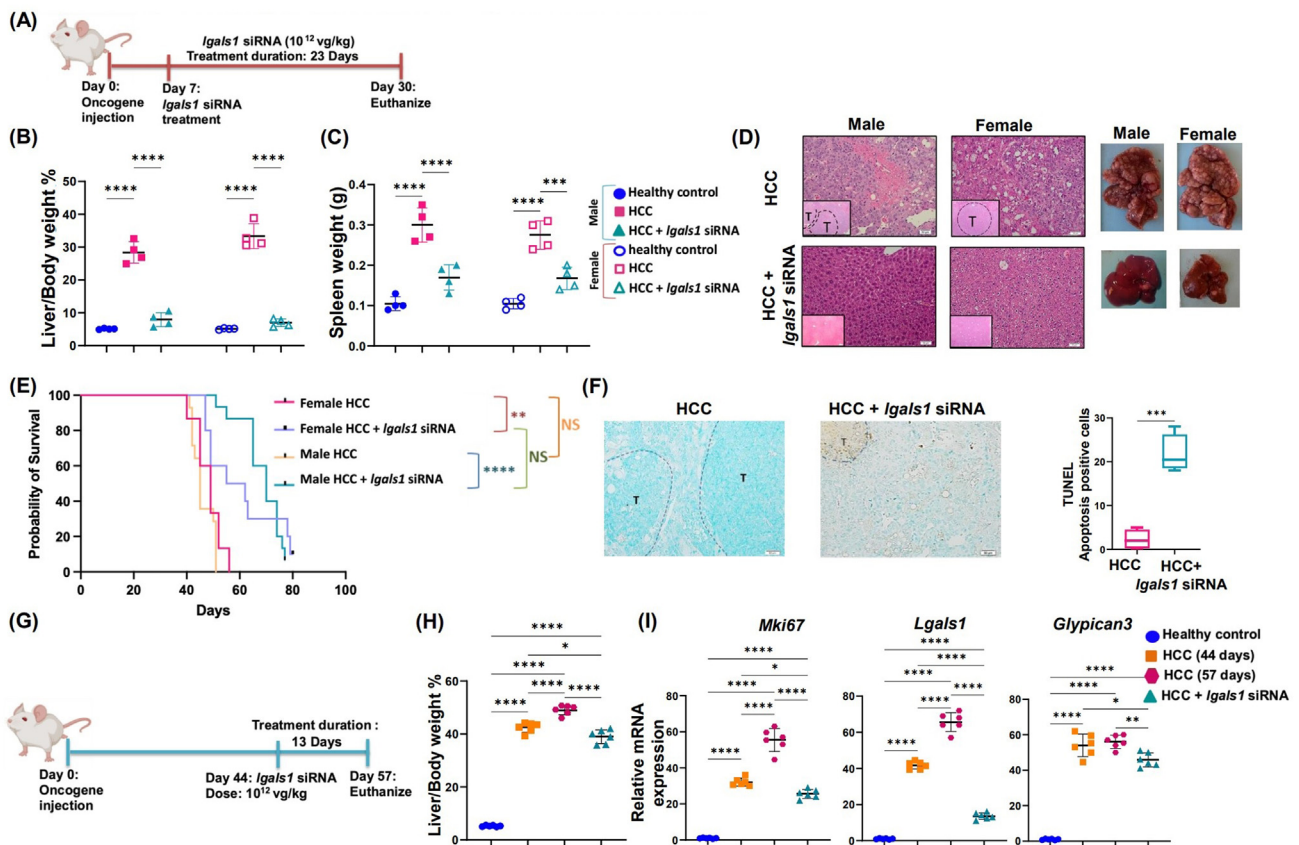
Figure 3 Gal1 silencing treats HCC and prolongs overall survival. (A) Experimental scheme. HCC mice of both sexes were treated with *lgals1* siRNA 7 days after myr-Akt1 and N-RasV12 injection and euthanized 30 days later (*n* = 4/group). (B) Liver to body weight ratio. (C) Spleen weight. (D) H&E-stained liver sections (magnification 400 × or 40 ×). (E) Kaplan−Meier survival curves. Mice were euthanized when they were moribund, and the death date was recorded as the next day. Log-rank test was performed (*n* = 11−14/group). (F) TUNEL assay staining. Nuclei stained with the TUNEL assay are brown. Sections were counterstained with Methyl Green. The percentage of positive TUNEL apoptosis-positive cells. (G) Experimental scheme. Male mice were treated with *lgals1* siRNA 44 days after myr-Akt1 and N-RasV12 injection and euthanized 57 days later (*n* = 6/group). (H) Liver to body weight ratio. (I) Relative mRNA levels of HCC markers. Data are shown as mean ± SD (*n* = 4−6/ group). ANOVA, Tukey, was used; *$P < 0.05$; **$P < 0.01$; ***$P < 0.001$; ****$P < 0.0001$.

lgals1-OE. Transcriptomic profiles were also compared in human HCC patients who had low or high Gal1 expression levels. Furthermore, spatial RNA sequencing was performed to identify location-specific events. The hepatic tissues used were from HCC mice treated with *lgals1* siRNA or *lgals1*-OE, 7 days post oncogene injection (Fig. 4A).

3.5.   Signaling pathways based on transcriptomic profiling

Principal component analysis revealed 4 distinct clusters that differentiated the healthy livers, HCC, *lgals1*-OE, and *lgals1* siRNA (Supporting Information Fig. S6A). Compared with the healthy livers, HCC had increased HCC markers, including *Afp* (110-fold), *Gp3* (40-fold), *Lgals1* (24-fold), *Cd44* (15-fold), *Cd133* (10-fold), and Collagen 4a1 (12-fold, bar graphs not shown), indicating the presence of inflammation and fibrosis in addition to HCC (bar graphs not shown).

Comparing HCCs with healthy livers, there were 4997 differentially expressed genes (DEGs; FDR-adjusted $P \leq 0.05$). The number of DEGs in *lgals1* siRNA treated *vs.* HCC was 4695. The differentially enriched pathways are shown in Fig. S3B and S3C. The healthy livers and *lgals1* siRNA-treated HCC commonly had enriched metabolic pathways for bile acid, fatty acid, xenobiotics,

and oxidative phosphorylation, among others revealing intact or improved liver function. In contrast, HCC had enriched G2M, EMT, hypoxia, inflammation, P53, etc. (Fig. S6B and S6C). Moreover, the same pathways were found to be differentially enriched when *lgals1* siRNA-treated HCCs were compared with the OE group (Fig. 4B).

To demonstrate human relevance, significantly enriched pathways in Gal1 low *vs.* high human HCC were studied. Human HCC data were obtained from the UCSC Xena (http://xena.ucsc.edu/), which includes 41 *LGALS1* high and 39 *LGALS1* low HCC patients' data (Fig. 4C). The analyses revealed that there were 9 pathways commonly enriched in high Gal1 human and mouse HCCs (EMT signaling pathway, apical junction, inflammatory response, KRAS signaling UP, allograft rejection, P53 pathway, myogenesis, TNF-α signaling *via* NF-κB, and IL2/STAT5 signaling). In contrast, the commonly enriched pathways found in low Gal1 human and mouse HCCs were bile acid, fatty acid, xenobiotic, heme metabolisms, peroxisome, and adipogenesis (Fig. 4B−D).

3.6.   Specific Gal1 targeted pathways based on location

Spatial RNA sequencing was performed to study location-specific events targeted by Gal1. The selected region of interest (ROI)
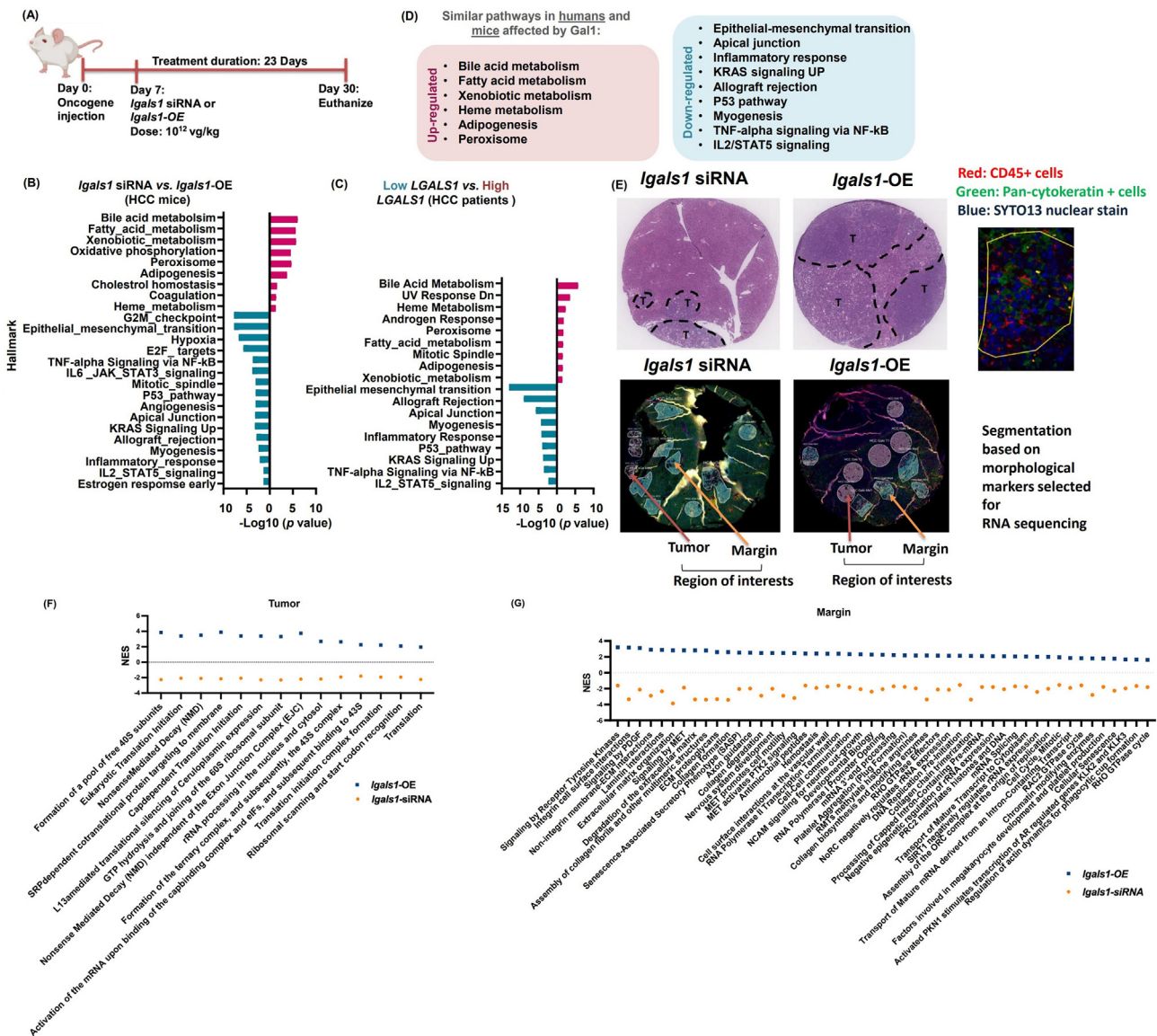
Figure 4 Gal1 silencing reverses the signaling that is enriched due to carcinogenesis. (A) Experimental scheme. Male mice were treated with either *lgals1* siRNA or *lgals1*-OE, seven days after myr-Akt1 and N-RasV12 injection and were euthanized 30 days later (*n* = 5/group). (B) *lgals1* siRNA (low-Gal1) compared to *lgals1*-OE (high-Gal1) in mouse HCC. (C) Enriched pathways in HCC patients with low *vs.* high *LGALS1* levels. A positive (upregulated) normalized enrichment score (NES) value is in red, and the negative (downregulated) NES is in blue. (D) The same up and down-regulated pathways were found in mice and human HCC based on Gal1 expression level (*n* = 3−4). (E) An example of selecting a region of interest (ROI) and further segmentation to select the area of interest illumination of interest (AOI) based on markers CD45 or pan-cytokeratin. (F, G) Pathways (based on Reactome) that significantly changed in opposite directions due to Gal1 silencing and OE in the tumors and at the margin of CD45$^+$ cells. The significant enrichment was considered at FDR<25%.

included tumors or tumor-margins (Fig. 4E). Transcriptomics pathway analysis revealed location-specific effects. Inside the tumors, compared with healthy livers, many specific upregulated pathways were related to cell division/cycle or RNA transcription. However, at tumor margins, specific pathways found were related to matrix formation, cell junction organization, recognition of foreign antigens, and metabolic pathways (Supporting Information Table S3).

Segmentation was done to select areas of illumination for RNA sequencing. This was done based on morphological markers of CD45 or pan-cytokeratin within each ROIs (Fig. 4E). We focused on CD45$^+$ cells because of the immunoregulatory roles of Gal1. In

addition, in healthy livers, CD45$^+$ cells are the minority cell population (5%−15%) in contrast to hepatocytes (60%−80%)[30,31]. Thus, the significance of CD45$^+$ cells might not be apparent when bulk RNA sequencing data were used. In addition, we focused on the pathways commonly altered by silencing and OE in the opposite direction, *i.e.*, Gal1-specific signaling.

For CD45$^+$ cells within the tumors, Gal1 silencing down-regulated 14 pathways (orange dots), which were all upregulated by Gal1 OE (blue dots, Fig. 4F). All those pathways are related to the process of translation, and the pathways can be roughly divided into three stages of translation, *i.e.*, initiation, elongation, and termination[32,33]. The pathways implicated in initiations are (1) formation of

a pool of free 40S subunit, (2) signal recognition particle (SRP)-dependent translational protein targeting to membrane, (3) cap-dependent translation initiation, (4) L13 mediated translational silencing of ceruloplasmin expression, (5) activation of the mRNA upon binding of the cap-binding complex and elFs, and subsequent binding to 43S, (6) formation of the ternary complex and subsequently, the 43S complex, (7) translation initiation complex formation, (8) ribosomal scanning and start codon recognition (9) eukaryotic translational initiation. The pathways related to elongation are GTP hydrolysis and joining of the 60S ribosomal subunit and translation. Additionally, the pathways involved in termination are nonsense-mediated decay and Nonsense-mediated decay independent of the exon junction complex.

At the tumor-margin, Gal1 silencing inhibited 49 pathways, which were all upregulated due to Gal1-OE (Fig. 4G). Based on their biological functions, those pathways regulate (1) cell signaling and communication, (2) extracellular matrix organization and degradation, (3) regulation of actin dynamics for phagocytic cup formation (refers to the process by which a cell reshapes its plasma membrane and cytoskeleton to form a "cup" that engulfs a particle or microorganism), (4) antimicrobial defense, (5) RNA transcription and processing, (6) chromatin modification, (7) cell cycle regulation, (8) cellular senescence, (9) megakaryocyte development and platelet production, etc.

For pan-cytokeratin + cells, the uncovered pathways were similar to those generated using bulk RNA sequencing mentioned above. However, it is fascinating to note that the same pathways that regulate translation initiation, elongation, and termination within the tumors were also found in pan-cytokeratin + cells inside the tumors. Together, Gal1 has a significant impact in regulating translational processes within the tumor, irrespective of the cell type.

3.7. The therapeutic effect of Gal1 silencing is CD8 T cell-dependent

Because Gal1 can modulate the activation of T cells by binding to their surface receptors and promoting or inhibiting their activation[4−8], we questioned whether the induction of cytotoxic T cells might account for the anti-HCC effects of *lgals1* siRNA. The enrichment scores of CD8$^+$ T cell subtypes were quantified by spatial deconvolution, which is a robust computational program used to determine the enrichment score or abundance of different cell types within a spatial location. In response to *lgals1* siRNA treatment, the score for immune infiltration, which represents the number of all types of immune cells, was elevated in both tumor and margin (higher in tumor than margin, Fig. 5A). Within the tumor, Gal1 silencing uniquely enriched cytotoxic T cells and central memory CD8$^+$ T cells but did not change the abundance of effector memory cells, exhausted cells, and naïve CD8$^+$ cells (Fig. 5B). However, at the tumor-margin, Gal1 silencing specifically increased the abundance of effector memory CD8$^+$ T cells, which play a pivotal role in providing rapid and effective protection against foreign antigens that have been previously exposed.

To further examine the significance of cytotoxic T cells in contributing to the anti-HCC effects of *lgals1* siRNA, mice were treated with anti-CD8 specific antibodies to deplete CD8$^+$ cells. Control mice received isotype control antibodies. The treatments continued throughout the entire experiment, and depletion was confirmed by IHC (data not shown). The experimental scheme is summarized in Fig. 5C.

The data showed that depleting CD8$^+$ cells did not affect tumor load (Fig. 5D), which was consistent with published findings[34]. However, depleting CD8$^+$ cells abolished the anti-HCC effects of *lgals1* siRNA based on the tumor load, spleen weight (Fig. 5D), as well as histology (not shown). In addition, enzyme-linked immunosorbent assay showed that CD3$^+$ T cells isolated from the livers of *lgals1* siRNA-treated mice were able to produce much higher concentrations of IFNγ and Gramzyme B compared with those isolated from untreated HCC mice, revealing their cytotoxic effect (Fig. 5E).

4. Discussion

This is the first study that uncovers the therapeutic potential of silencing Gal1 using AAV9, which can prevent and treat HCC in both genders. Thus, Gal1 is not only an HCC biomarker but also a target for prevention as well as treatment. The prevention effect is further supported by its effects in reducing fibrosis and inhibiting EMT. The findings have translational potential because AAV is a preferred platform due to its sustained impact and safety profile[35]. AAV9 is also approved by the FDA[36]. A study revealed that i.v. injection of AAV9 is sufficient for "lifetime" transgene expression for the treatment of spinal muscular atrophy[37]. The liver tropism effect was also shown in our study[38]. Moreover, this one-dose treatment did not produce noticeable toxic effects based on gross morphology, toxicity tests, and blood counts.

The human relevance of the presented findings has been revealed in the current preclinical model. The expression levels of Gal1 were elevated in HCC and further escalated when tumors were in the advanced stage. Additionally, Gal1 levels predict survival outcomes. In mice, prior to tumor initiation, forced expression of Gal1 increased tumor load in contrast to reduction due to silencing. Those findings support the essential roles of Gal1 in liver carcinogenesis. The human relevance of the findings was also revealed by comparing high and low Gal1 expressing HCCs in human patients. The same molecular pathways related to inflammation, EMT, and oncogenic signaling are enriched due to elevated Gal1. In contrast, improved hepatic metabolism was revealed when Gal1 levels were low in both humans and mice.

The spatial transcriptomic data provided location-specific information to differentiate the roles of Gal1 based on biomarkers. CD45, which is found in immune cells, is a transmembrane tyrosine phosphatase that plays a role in regulating matrix formation. Specifically, CD45$^+$ cells interact with fibroblasts and myofibroblasts through cytokines such as TGFβ, and direct cell−cell contact *via* integrin-mediated adhesion, which promotes ECM formation[39,40]. Additionally, CD45$^+$ cells secrete matrix metalloproteinases to degrade ECM components and facilitate tissue remodeling[41]. CD45$^+$ immune cells also regulate the activity of matrix metalloproteinases by producing tissue inhibitors of metalloproteinases[40,42]. The spatial transcriptomic generated pathways, which shifted in opposite directions due to OE and silencing, clearly revealed that Gal1 significantly impacts the roles of CD45$^+$ cells in matrix formation at the tumor margin. The uncovered pathways are extensive and range from integrin cell surface interactions, non-integrin membrane−ECM interactions, laminin interactions, extracellular matrix organization, assembly of collagen fibrils and other multimeric structures, ECM proteoglycans, collagen formation, and collagen degradation. It would be interesting to investigate further the binding of Gal1 to specific matrix proteins at the tumor margin, leading to those processes being changed.
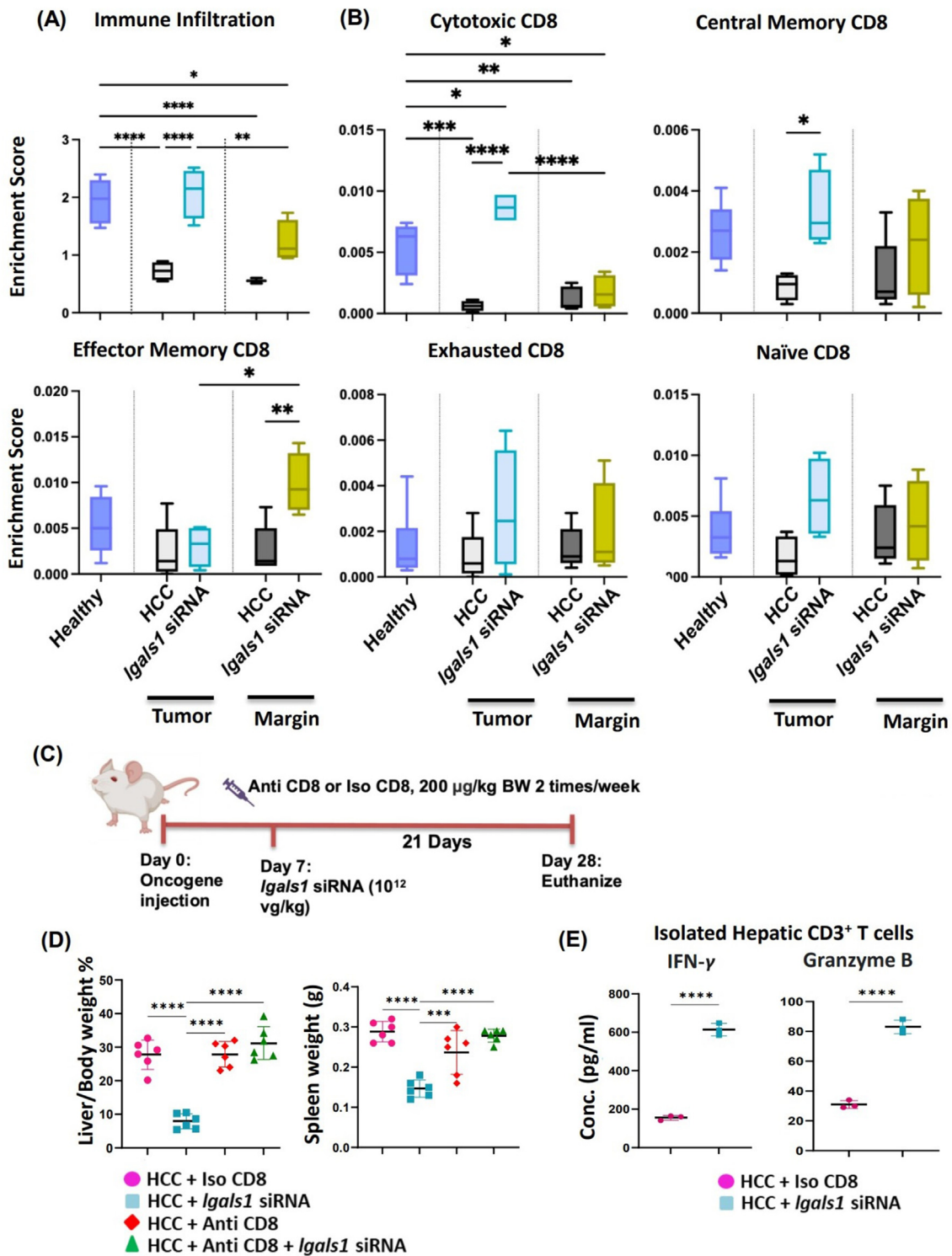
Figure 5 The therapeutic effect of silencing Gal1 is CD8 T cell-dependent. (A) Infiltration score of CD45$^+$ cells in the tumors and at the tumor margins. (B) Normalized enrichment score of CD8$^+$ T cells subtypes in the tumors and margins. (C) Experimental scheme. Mice were treated with *lgals1* siRNA 7 days after Akt/Ras-induced HCC and/or with anti-CD8 antibodies ($n = 5-6$/group) or iso CD8 (200 μg/kg BW, i.p., 2 times/week), then euthanized 28 days later. (D) Liver to body weight ratio and spleen weight. (E) The concentrations of IFN-gamma (IFN-γ, pg/mL) and granzyme B (pg/mL) produced by isolated hepatic CD3$^+$ T cells (3 mice/group). Data are shown as mean ± SD (3−6 mice/group). ANOVA, Tukey, was used; *$P < 0.05$; **$P < 0.01$; ***$P < 0.001$; and ****$P < 0.0001$.

At the tumor margin, another significant signaling induced by *lgals1*-OE but reduced by Gal1 silencing is related to the recognition of foreign antigens. Those pathways include (1) antimicrobial peptides, (2) cell surface interactions at the vascular wall, which include recognition of pathogens and activation of immune responses, (3) platelet aggregation, which plays a key role in the recognition and response to injury and foreign pathogens, (4) regulation of actin dynamics for phagocytic cup formation, (5) RAC2 GTPase cycle, which plays in recognition and destruction of foreign pathogens. These findings unequivocally demonstrated the immunosuppressive roles of Gal1 at the tumor margin. Furthermore, in a xenograft mouse model, silencing Gal1 in carcinomas-associated fibroblasts reduces HCC progression[43]. It is intriguing to note that, in response to Gal1 silencing, the effector memory CD8^{+} T cells expanded at the tumor margin while inflammation-driven EMT was inhibited, which generated anti-HCC effects.

Our novel data uncovered the significance of Gal1 in regulating translation inside the tumors. Gal1 also has been shown to interact with mRNAs with a preference for binding to close-to-stop codons, thereby regulating angiogenesis[44]. It is interesting to note that hypoxia is a known factor that induces Gal1[45]. While hypoxia-inducible factors regulate transcription, including stimulating Gal1 expression[46], Gal1 binding might further regulate translation processing in tumorigenesis. The information related to how Gal1 regulates translation remains limited. The data generated in the current study uncovered the potential extensive roles of Gal1 in translation initiation, elongation, as well as termination stressing its significance, which warrants further investigation.

5. Conclusions

Taken together, Gal1 is not only an HCC biomarker; it predicts HCC patient survival outcomes. Targeting Gal1 is effective in preventing as well as treatment of HCC and has translational potential. The mechanisms of action can be many. Silencing Gal1 reduces EMT and matrix formation at the tumor margin and provocates the infiltration of immune cells as well as the expansion of cytotoxic T cells. Moreover, silencing Gal1 inhibits the translational machinery within the tumor. Those changes contributed to the anti-HCC effects of Gal1 silencing gene therapy.

Author contributions

Conceptualization, methodology, and study design: Yu-Jui Yvonne Wan and Tahereh Setayesh; Resources: Ying Hu, Farzam Vaziri, Tahereh Setayesh, Yu-Jui Yvonne Wan; Data acquisition, data analysis, and interpretation: Tahereh Setayesh, Farzam Vaziri, Ying Hu, Xin Chen, Jinping Lai, and Dongguang Wei; Writing - Original Draft: Tahereh Setayesh, Yu-Jui Yvonne Wan; Review & Editing: All authors; Visualization: Yu-Jui Yvonne Wan and Tahereh Setayesh; Funding acquisition: Yu-Jui Yvonne Wan and Tahereh Setayesh, Ying Hu.

Conflicts of interest

The authors declare no potential competing interests.

Appendix A.   Supporting information

Supporting data to this article can be found online at https://doi.org/10.1016/j.apsb.2023.10.010.

References

1. Ferlay J, Colombet M, Soerjomataram I, Parkin DM, Piñeros M, Znaor A, et al. Cancer statistics for the year 2020: an overview. *Int J Cancer* 2021;**149**:778−89.
2. Colquhoun SD, Wan YY. Hepatocellular carcinoma diagnosis and treatment: an overview. *Liver Res* 2020;**4**:159−60.
3. Yang JD, Hainaut P, Gores GJ, Amadou A, Plymoth A, Roberts LR. A global view of hepatocellular carcinoma: trends, risk, prevention and management. *Nat Rev Gastroenterol Hepatol* 2019;**16**:589−604.
4. Perillo NL, Pace KE, Seilhamer JJ, Baum LG. Apoptosis of T cells mediated by galectin-1. *Nature* 1995;**378**:736−9.
5. Setayesh T, Colquhoun SD, Wan YY. Overexpression of galectin-1 and galectin-3 in hepatocellular carcinoma. *Liver Res* 2020;**4**:173−9.
6. Rabinovich GA, Toscano MA. Turning 'sweet' on immunity: galectin−glycan interactions in immune tolerance and inflammation. *Nat Rev Immunol* 2009;**9**:338−52.
7. Cedeno-Laurent F, Dimitroff CJ. Galectin-1 research in T cell immunity: past, present and future. *Clin Immunol* 2012;**142**:107−16.
8. Liu FT, Rabinovich GA. Galectins as modulators of tumour progression. *Nat Rev Cancer* 2005;**5**:29−41.
9. Spano D, Russo R, Di Maso V, Rosso N, Terracciano LM, Roncalli M, et al. Galectin-1 and its involvement in hepatocellular carcinoma aggressiveness. *Mol Med* 2010;**16**:102−15.
10. Rabinovich GA. Galectin-1 as a potential cancer target. *Br J Cancer* 2005;**92**:1188−92.
11. Cagnoni AJ, Giribaldi ML, Blidner AG, Cutine AM, Gatto SG, Morales RM, et al. Galectin-1 fosters an immunosuppressive microenvironment in colorectal cancer by reprogramming CD8^{+} regulatory T cells. *Proc Natl Acad Sci U S A* 2021;**118**:e2102950118.
12. Leung Z, Ko FCF, Tey SK, Kwong EML, Mao X, Liu BHM, et al. Galectin-1 promotes hepatocellular carcinoma and the combined therapeutic effect of OTX008 galectin-1 inhibitor and sorafenib in tumor cells. *J Exp Clin Cancer Res* 2019;**38**:423.
13. Bacigalupo ML, Manzi M, Espelt MV, Gentilini LD, Compagno D, Laderach DJ, et al. Galectin-1 triggers epithelial-mesenchymal transition in human hepatocellular carcinoma cells. *J Cell Physiol* 2015;**230**:1298−309.
14. Chong Y, Tang D, Xiong Q, Jiang X, Xu C, Huang Y, et al. Galectin-1 from cancer-associated fibroblasts induces epithelial−mesenchymal transition through β1 integrin-mediated upregulation of Gli1 in gastric cancer. *J Exp Clin Cancer Res* 2016;**35**:175.
15. Tang D, Gao J, Wang S, Ye N, Chong Y, Huang Y, et al. Cancer-associated fibroblasts promote angiogenesis in gastric cancer through galectin-1 expression. *Tumour Biol* 2016;**37**:1889−99.
16. Zhang P, Li K, Shen Y, Gao P, Dong Z, Cai J, et al. Galectin-1 induces hepatocellular carcinoma EMT and sorafenib resistance by activating FAK/PI3K/AKT signaling. *Cell Death Dis* 2016;**7**:e2201.
17. Potikha T, Pappo O, Mizrahi L, Olam D, Maller SM, Rabinovich GA, et al. Lack of galectin-1 exacerbates chronic hepatitis, liver fibrosis, and carcinogenesis in murine hepatocellular carcinoma model. *Faseb J* 2019;**33**:7995−8007.

18. Wang L, Wan YY. The role of gut microbiota in liver disease development and treatment. *Liver Res* 2019;**3**:3−18.

19. Jena PK, Sheng L, Nagar N, Wu C, Barile D, Mills DA, et al. Synbiotics bifidobacterium infantis and milk oligosaccharides are effective in reversing cancer-prone nonalcoholic steatohepatitis using western diet-fed FXR knockout mouse models. *J Nutr Biochem* 2018;**57**:246−54.

20. Maurya S, Sarangi P, Jayandharan GR. Safety of adeno-associated virus-based vector-mediated gene therapy—impact of vector dose. *Cancer Gene Ther* 2022;**29**:1305−6.

21. Ho C, Wang C, Mattu S, Destefanis G, Ladu S, Delogu S, et al. AKT (v-akt murine thymoma viral oncogene homolog 1) and N-Ras (neuroblastoma ras viral oncogene homolog) coactivation in the mouse liver promotes rapid carcinogenesis by way of mTOR (mammalian target of rapamycin complex 1), FOXM1 (forkhead box M1)/SKP2, and c-Myc pathways. *Hepatology* 2012;**55**:833−45.

22. Hu Y, Zhan Q, Liu HX, Chau T, Li Y, Wan YJ. Accelerated partial hepatectomy-induced liver cell proliferation is associated with liver injury in Nur77 knockout mice. *Am J Pathol* 2014;**184**:3272−83.

23. Ha SY, Choi M, Lee T, Park CK. The prognostic role of mitotic index in hepatocellular carcinoma patients after curative hepatectomy. *Cancer Res Treat* 2016;**48**:180−9.

24. Hu Y, Setayesh T, Vaziri F, Wu X, Hwang ST, Chen X, et al. miR-22 gene therapy treats HCC by promoting anti-tumor immunity and enhancing metabolism. *Mol Ther* 2023;**31**:1829−45.

25. Gyamfi MA, He L, French SW, Damjanov I, Wan YJ. Hepatocyte retinoid X receptor alpha-dependent regulation of lipid homeostasis and inflammatory cytokine expression contributes to alcohol-induced liver injury. *J Pharmacol Exp Therapeut* 2008;**324**:443−53.

26. Miao YR, Xia M, Luo M, Luo T, Yang M, Guo AY. ImmuCellAI-mouse: a tool for comprehensive prediction of mouse immune cell abundance and immune microenvironment depiction. *Bioinformatics* 2022;**38**:785−91.

27. Miao YR, Zhang Q, Lei Q, Luo M, Xie GY, Wang H, et al. ImmuCellAI: a unique method for comprehensive T-cell subsets abundance prediction and its application in cancer immunotherapy. *Adv Sci* 2020;**7**:1902880.

28. Chai ZT, Zhang XP, Shao M, Ao JY, Chen ZH, Zhang F, et al. Impact of splenomegaly and splenectomy on prognosis in hepatocellular carcinoma with portal vein tumor thrombus treated with hepatectomy. *Ann Transl Med* 2021;**9**:247.

29. Kyrylkova K, Kyryachenko S, Leid M, Kioussi C. Detection of apoptosis by TUNEL assay. *Methods Mol Biol* 2012;**887**:41−7.

30. Heymann F, Tacke F. Immunology in the liver—from homeostasis to disease. *Nat Rev Gastroenterol Hepatol* 2016;**13**:88−110.

31. Crispe IN. The liver as a lymphoid organ. *Annu Rev Immunol* 2009;**27**:147−63.

32. Jackson RJ, Hellen CUT, Pestova TV. The mechanism of eukaryotic translation initiation and principles of its regulation. *Nat Rev Mol Cell Biol* 2010;**11**:113−27.

33. Hinnebusch AG. The scanning mechanism of eukaryotic translation initiation. *Annu Rev Biochem* 2014;**83**:779−812.

34. Wen L, Xin B, Wu P, Lin CH, Peng C, Wang G, et al. An efficient combination immunotherapy for primary liver cancer by harmonized activation of innate and adaptive immunity in mice. *Hepatology* 2019;**69**:2518−32.

35. Maurya S, Sarangi P, Jayandharan GR. Safety of adeno-associated virus-based vector-mediated gene therapy—impact of vector dose. *Cancer Gene Ther* 2022;**29**:1305−6.

36. Shahryari A, Saghaeian Jazi M, Mohammadi S, Razavi Nikoo H, Nazari Z, Hosseini ES, et al. Development and clinical translation of approved gene therapy products for genetic disorders. *Front Genet* 2019;**10**:868.

37. Al-Zaidy S, Pickard AS, Kotha K, Alfano LN, Lowes L, Paul G, et al. Health outcomes in spinal muscular atrophy type 1 following AVXS-101 gene replacement therapy. *Pediatr Pulmonol* 2019;**54**:179−85.

38. Sands MS. AAV-mediated liver-directed gene therapy. *Methods Mol Biol* 2011;**807**:141−57.

39. Kisseleva T, Brenner D. Molecular and cellular mechanisms of liver fibrosis and its regression. *Nat Rev Gastroenterol Hepatol* 2021;**18**:151−66.

40. Rheinländer A, Schraven B, Bommhardt U. CD45 in human physiology and clinical medicine. *Immunol Lett* 2018;**196**:22−32.

41. Sorokin L. The impact of the extracellular matrix on inflammation. *Nat Rev Immunol* 2010;**10**:712−23.

42. Bourboulia D, Stetler-Stevenson WG. Matrix metalloproteinases (MMPs) and tissue inhibitors of metalloproteinases (TIMPs): positive and negative regulators in tumor cell adhesion. *Semin Cancer Biol* 2010;**20**:161−8.

43. Tsai YT, Li CY, Huang YH, Chang TS, Lin CY, Chuang CH, et al. Galectin-1 orchestrates an inflammatory tumor-stroma crosstalk in hepatoma by enhancing TNFR1 protein stability and signaling in carcinoma-associated fibroblasts. *Oncogene* 2022;**41**:3011−23.

44. Wei J, Li DK, Hu X, Cheng C, Zhang Y. Galectin-1−RNA interaction map reveals potential regulatory roles in angiogenesis. *FEBS Lett* 2021;**595**:623−36.

45. Le Q-T, Shi G, Cao H, Nelson DW, Wang Y, Chen EY, et al. Galectin-1: a link between tumor hypoxia and tumor immune privilege. *J Clin Oncol* 2005;**23**:8932−41.

46. Chee NT, Lohse I, Brothers SP. mRNA-to-protein translation in hypoxia. *Mol Cancer* 2019;**18**:49.